Available online at www.sciencedirect.com

SciVerse ScienceDirect

Energy Procedia 37 (2013) 4473 – 4482

Energy Procedia

GHGT-11

Does injected CO_2 affect (chemical) reservoir system integrity? – A comprehensive experimental approach

Sebastian Fischer[a,b,*], Axel Liebscher[a], Kornelia Zemke[a], Marco De Lucia[a], and the Ketzin Team

[a]*Helmholtz Centre Potsdam, GFZ German Research Centre for Geosciences, Centre for CO_2 Storage, Potsdam, Germany*
[b]*Berlin Institute of Technology, School VI, Department of Applied Geosciences, Chair of Mineralogy-Petrology, Berlin, Germany*

Abstract

In order to investigate and characterize single fluid-mineral interactions we successfully implemented a new hydrothermal laboratory. CO_2-exposure experiments using separates of rock-forming minerals were performed on a hydrothermal rocking autoclave. The system is equipped with flexible Titanium cells allowing for isobaric sampling. Experiments were run for one week at 80 °C and 20 MPa/30 MPa. Rietveld refined XRD data reveal that the initial siderite separate is composed of 69.6±1.3 wt% siderite, 26.7±1.2 wt% ankerite and 3.8±0.8 wt% quartz, respectively. Over time, siderite abundances increase and ankerite abundances correspondingly decrease, while quartz abundances are constant within error. Fluid data show rapid increases for Ca^{2+}, Mg^{2+}, Mn^{2+} and Fe^{2+}. After these rapid increases, Ca^{2+} and Mg^{2+} reveal slight decreases that are followed by subsequent rises to maximum concentrations at the end of the experiments, while Mn^{2+} and Fe^{2+} decrease continuously after the initial maxima. SEM micrographs of CO_2-exposed samples indicate dissolution of ankerite, while siderite and quartz are mainly unaffected. The experiments on the siderite separate clearly show that ankerite is dissolved and siderite is stable. We conclude that siderite is a potential CO_2 trapping phase in iron-bearing reservoirs.

Selection and/or peer-review under responsibility of GHGT

Keywords: batch experiments; separates of rock-forming minerals; sandstone and siltstone samples

* Corresponding author: Sebastian Fischer. Tel.: +49 (0)331 288 28 37.
E-mail address: fischer@gfz-potsdam.de.

1876-6102
Selection and/or peer-review under responsibility of GHGT
doi:10.1016/j.egypro.2013.06.352

1. Introduction

Static batch experiments have been performed to investigate mineralogical and geochemical effects of CO_2 exposure on whole rock core samples from the Ketzin pilot site. Powdered monomineralic separates were used to conduct complementary laboratory experiments in order to be able (i) to characterize single fluid-mineral interactions in a relatively simple system, (ii) to assign individual reactions to one mineral and (iii) to calculate dissolution rates for individual rock-forming minerals. In addition, potential mineral precipitates should be easier detectable in these monomineralic experiments.

The first two sets of long term CO_2-exposure experiments were performed on reservoir and cap-rock-like core material from the pilot CO_2 storage site at Ketzin. Reservoir sandstone samples were exposed to pure CO_2 and synthetic reservoir brine at near in-situ P-T conditions (40°C, 5.5 MPa) for a maximum of 40 months (Exp-A). In a second approach, cap-rock-like siltstone samples were exposed to pure CO_2 and synthetic reservoir brine at 40°C and 7.5 MPa for a maximum of six months (Exp-B). Results of Exp-A were presented and discussed in [1] and [2]. To complete the experimental investigations of mineralogical-geochemical interactions likely to occur within a storage system, siderite was chosen to react with pure CO_2 and 2 M NaCl brine in a new hydrothermal rocking autoclave system equipped with flexible Titanium cells. In this paper we focus on the monomineralic experiments using siderite (Exp-C1) and we will only briefly refer to results of Exp-A and Exp-B.

2. Materials and Methods

2.1 Sample Description

The monomineralic siderite (iron carbonate) separate used for the experimental series (Exp-C) was received from BRG Hannover and prepared according to procedures described in [3]. Siderite was crushed and sieved to arrive at a grain size fraction of 100 to 200 µm. Based on [3], XRD data with Rietveld refinement prove that the siderite separate is composed of 80 wt% siderite, 17 wt% ankerite and 3 wt% quartz. As determined by EDS multipoint data, the formula of siderite is $Fe_{0.8}Mg_{0.1}Mn_{0.1}CO_3$, that of ankerite is $Ca(Mg_{0.2}Mn_{0.1}Fe_{0.8})(CO_3)_2$; in siderite, Mn^{2+} contents correlate with those of Fe^{2+} [3].

2.2 Experimental Approach

The experiments using monomineralic separates were performed on a new hydrothermal rocking autoclave system equipped with flexible Titanium Grade-2 cells (Fig. 1). Confining pressure was generated and controlled with an air driven fluid pump (Confining Pressure Controller). During heat up, sampling and/or cooling the pressure was held constant using a backpressure regulator.

Approximately 5.5 g of the powdered mineral separate were filled into the flexible Ti-cell, which had a volume of about 150 ccm. The Ti-cell was then completely filled with 2 M NaCl and attached to the autoclave vessel, which was then loaded into the oven. The 2 M NaCl brine was prepared using Sigma-Aldrich NaCl salt powder with a purity of $\geqslant$99.5%. After all pressure connections were tested for tightness, the system was set to 8.0 MPa. The Ti-cell valve was then cautiously opened to take out a pre-calculated brine volume. Next, an industrial CO_2 flask (at a pressure of approximately 6.0 MPa) was connected with the Ti-cell valve and CO_2 was added to the Ti-cell by lowering the autoclave pressure slowly below that of the CO_2 flask (below 6.0 MPa) using the backpressure regulator. A measuring cylinder was put under the overflow pipe of the autoclave to control the added CO_2 volume, which was sufficient to guarantee for excess CO_2 during the course of the experiment. It was assumed that the volume of displaced water from the autoclave equals the loaded CO_2 volume. Next, the Ti-cell valve was

tightly closed. Afterwards, the system was pressurized to 20 MPa/30 MPa and heated to 80 °C thereafter. For heating, the backpressure regulator was set to experimental pressure. Displaced water was collected in an external reservoir and the autoclave as well as the loaded Ti-cell were isobaric at all times. For each individual experiment, the brine to mineral weight-ratio was 20 to one. During sampling, the oven unit was turned upside down to assure sampling of brine instead of CO_2 fluid from the headspace. Sampling was performed by setting the air pump slightly above 20 MPa/30 MPa so that, once brine fluid left the Ti-cell, water could flow into the autoclave to keep the system isobaric. In order to determine time dependent dissolution behavior, successive fluid samples were taken after several different time steps. A total of 2.5 to 3.0 ml fluid were sampled for each sampling run; 1.0 ml out of the uptake, which was poured away, 1.0 ml for cation, and between 0.5 to 1.0 ml for anion analysis. Accordingly, the total amount of solution sampled (three to seven samples of 2.5 to 3.0 ml each in Exp-C1) did not exceed 12% of the initial solution volume. Sampling vials for cation analysis were acidified with 10 µl of 65% pure HNO_3. The pH was estimated using pH indicator paper, which was held directly at the Ti-cell valve outlet. Solid samples were washed out of the Ti-cell and filtered after quenching at the end of the run. Individual experiments were run for one week.

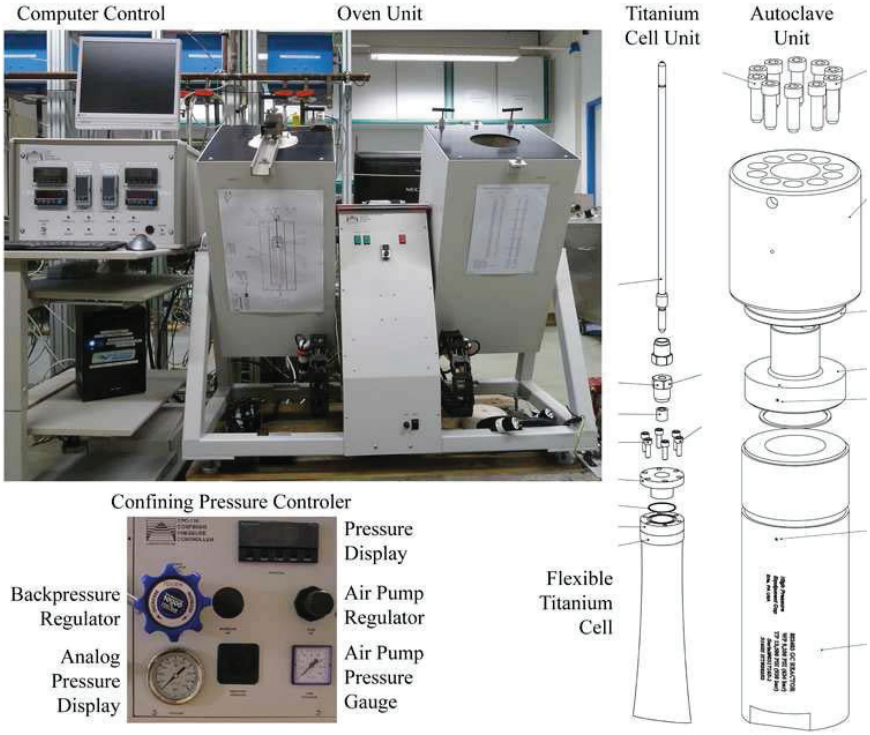

Fig. 1 – The hydrothermal rocking autoclave system used for the monomineralic experiments (Exp-C).

3. Analytical Techniques

3.1 Fluid Analysis

A DIONEX DX-120 ion chromatograph was used to determine Cl^- and SO_4^{2-} concentrations in the experimental brine. Deionized water was used for dilution to 1/100. Other anions were below detection limit. Cations were analyzed with a Varian VISTA-MPX ICP-AES device operating with axial plasma. Samples were diluted with deionized water to 1/100 for Mn^{2+}, Ba^{2+} and Sr^{2+}, 1/1,000 for Ca^{2+}, Mg^{2+} and Fe^{2+}, and 1/10,000 for Na^+. Sampled fluids were not additionally filtered because a filter was used with the Ti-cell adapter plug.

3.2 Analysis of Solid Material

In order to identify possible changes within each mineral and to be able to identify and quantify any new formed mineral phase(s), XRD measurements were performed on homogenized sample aliquots. Homogenization was done with an agate mortar and pestle; each sample aliquot was ground for ten minutes. X-ray diffraction data was collected on a Panalytical Empyrean diffractometer. Rietveld refinements were done with AutoQuan, a BGMN based software.

Selected samples were additionally investigated for changes of mineral surfaces with a Zeiss Ultra 55 plus Scanning Electron Microscope (SEM) equipped with an energy dispersive X-ray (EDS) system. The SEM was operated at 20 kV and 15 nA. Au-coatings were used to allow for carbonate detection and identification.

4. Results of Siderite Experiments

Until today three individual experiments using the siderite separate have been performed and evaluated; these are hereafter referred to as Exp-C1-1, Exp-C1-2 and Exp-C1-3, respectively. Exp-C1-1 was the first experiment conducted on the new rocking autoclave system. Due to problems related to the heating process and handling of the pump, anticipated experimental P-T conditions were reached only after 232 h (Fig. 2). Handling of the heat-up process was much better controlled and quicker for Exp-C1-2 and Exp-C1-3. The latter experiment was performed at 30 MPa. In the sampled brine, all three siderite experiments show generally increased ion concentrations for Ca^{2+}, Mg^{2+}, Mn^{2+} and Fe^{2+} with experimental run duration. Sr^{2+} was below detection limit in all samples. Na^+ was only measured in Exp-C1-1. In all the three siderite experiments, Ca^{2+} and Mg^{2+} as well as Fe^{2+} and Mn^{2+} concentrations, respectively, show similar behavior over time (Fig. 2).

In Exp-C1-1, Ca^{2+} and Mg^{2+} are steadily increasing to reach maximum concentrations of 1.62e-2 and 4.44e-3 mol/L after 576 h at the end of the experiment. Fe^{2+} and Mn^{2+} reach maximum concentrations of 1.22e-2 and 2.37e-4 mol/L after 312 h and continuously decrease from that moment on. Na^+ concentration levels are constant until 312 h and then decline slightly to a minimum of 1.78 mol/L after 456 h. To the end, Na^+ concentrations increase again slightly.

In Exp-C1-2, handling of the autoclave system was improved and the heat-up process was much quicker so that first samples could be taken about three hours after CO_2 addition. More samples were taken during the first hours of the experiment in order to have information of the phase of rapid concentration increase (which was not sampled in Exp-C1-1). Ca^{2+} and Mg^{2+} show a rapid increase and reach first maximum concentrations of 1.23e-2 and 3.67e-3 mol/L after 25 h. Both ions reveal decreasing concentrations to minima of 1.07e-2 and 3.38e-3 mol/L after 73 h. From that moment on, both ions continuously increase again to 1.21e-2 and 3.67e-3 mol/L at the end of the experiment. Fe^{2+} and Mn^{2+} also display similar behavior with the difference that after the maxima were reached during the initial

phase within 18 (Mn^{2+} = 4.27e-4) and 25 h (Fe^{2+} = 1.96e-3), respectively, both ions continuously decrease throughout the rest of the experiment.

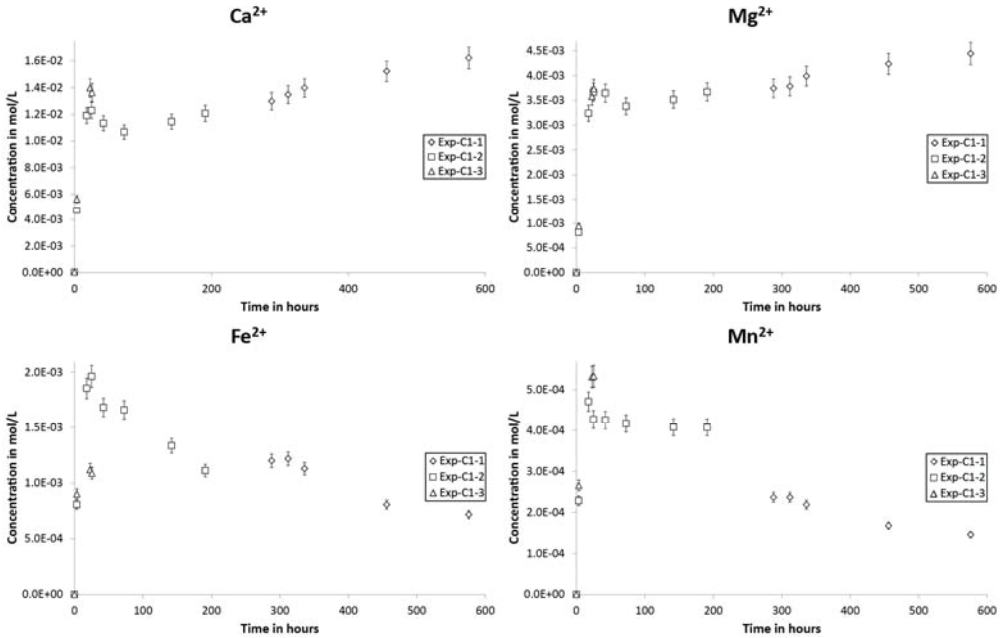

Fig. 2 – Fluid data for major cations from the three siderite experiments (Exp-C1-1, Exp-C1-2 and Exp-C1-3) plotted against experimental run duration. It is apparent that Ca^{2+} and Mg^{2+} as well as Fe^{2+} and Mn^{2+}, respectively, show similar behavior. Error bars plotted refer to 5% rel.

In Exp-C1-3, first samples were already taken four hours after CO_2 addition. In that time span, Ca^{2+}, Mg^{2+}, Mn^{2+} and Fe^{2+} increased rapidly. Ca^{2+} and Fe^{2+} concentrations reached maxima after 23 h (1.4e-2 and 1.1e-3 mol/L, respectively), while $Mg^{2+}$and Mn^{2+} concentrations continue to increase to the end of the experiment. Exp-C1-3 had to be stopped after approximately 30 h, because no more fluid could be sampled. It is assumed that the filter was blocked.

The comparison of Exp-C1-1, Exp-C1-2 and Exp-C1-3 reveals that the collected data for the siderite separate can be discussed and evaluated as one complete data set. In Figure 3 it is apparent that the quickest and highest initial concentration increases for Ca^{2+}, Mg^{2+} and Mn^{2+} generally occurred in Exp-C1-3, but also that Fe^{2+} concentrations in Exp-C1-3 are not as high as in Exp-C1-2. It is furthermore apparent that the comparatively late sampling but the longer run duration of Exp-C1-1 nicely completes the datasets of Exp-C1-2 and Exp-C1-3, respectively.

Mineral surfaces of grains from the untreated siderite separate as well as of Exp-C1-1 were studied with SEM. Quartz and traces of pyrite, K-feldspar and a K-rich clay mineral, possibly illite, were found next to siderite and ankerite. Untreated siderite shows surface structures that are characterized by relatively sharp edges and steps within the crystal, but also by fines and minor holes/kinks and pits occasionally (Fig. 3A). Surface structures on untreated ankerite (Fig. 3B) are very similar compared to untreated siderite. Nonetheless, siderite and ankerite grains can be clearly identified and differentiated optically and chemically. CO_2-treated ankerite grains show strongly corroded surface structures with

larger and much more frequent dissolution holes and pits (Fig. 3C+D), while some CO_2-treated siderite surfaces are less sharp-edged but reveal no change in quantity and depth of holes and pits (Fig. 4C).

Collected XRD diffractograms of the untreated siderite separate and the three siderite experiments reveal significant differences between the distinct samples; especially for the two carbonate phases. Siderite, ankerite and quartz were verified by XRD measurements. No new formed mineral phase was determined in any of the CO_2-treated samples. In Figure 4 it is apparent that siderite shows increasing modal abundances with time (from initially 69.6±1.3 to 80.7±1.5 wt% at the end), while ankerite shows the opposite trend (from initially 26.7±1.2 to 16.2±1.4 wt% at the end). Changes in quartz abundances are within analytical error (i.e. constant between 2.9±0.9 and 3.8±0.8 wt%). The untreated siderite separate is composed of 69.6±1.3 wt% siderite, 26.7±1.2 wt% ankerite and 3.8±0.8 wt% quartz. These mineral abundances slightly differ from those described in [3].

Experiments on illite and labradorite separates (Exps-C2 and Exps-C3) are still on-going and results will be at hand soon.

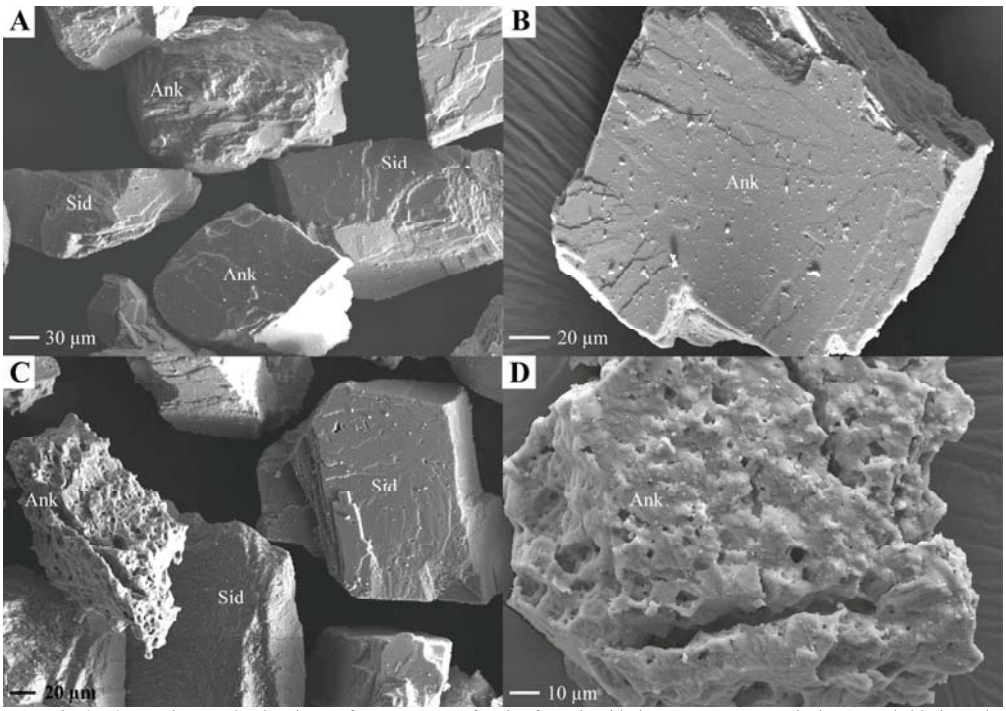

Fig. 3 – SEM micrographs showing surface structures of grains from the siderite separate. A – Typical untreated siderite and ankerite grains. B – Untreated ankerite grain with fines on the surface. C shows CO_2-treated grains of Exp-C1-1 that display some holes and pits on siderite surfaces, and strongly corroded ankerite surfaces. D – A CO_2-treated ankerite grain displaying typical dissolution features.

5. Discussion

The reaction of the siderite separate with CO_2 and 2 M NaCl brine is characterized by generally increased Ca^{2+}, Mg^{2+}, Mn^{2+} and Fe^{2+} concentrations. Optical and chemical grain inspection of the

untreated siderite separate reveals clear differentiation between siderite and ankerite, but also shows the presence of quartz, pyrite, K-feldspar and illite (?). The SEM investigation of grain surface morphologies additionally point towards higher solubility of ankerite over siderite under the applied experimental conditions. This is also supported by Rietveld refined XRD data, which reveal decreasing ankerite and increasing siderite abundances over time.

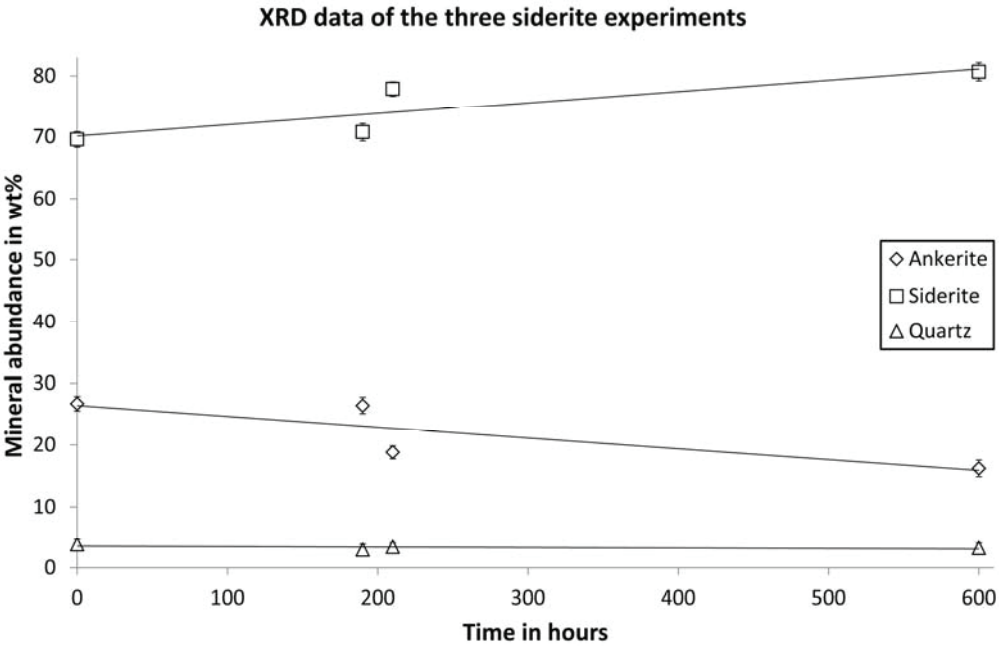

Fig. 4 – Mineral abundances plotted against time of CO_2 treatment. While quartz reveals constant abundances, siderite shows increasing and ankerite decreasing weight percentages over time, respectively. Error bars indicate relative errors for each refinement. 0 h refers to the untreated siderite separate, <200 h to Exp-C1-3, >200 h to Exp-C1-2, and 600 h to Exp-C1-1, respectively.

Despite the fact that Exp-C1-3 was conducted at 30 MPa, and Exp-C1-1 and Exp-C1-2 only at 20 MPa, respectively, we believe that – based on our data (Fig. 2) – all three siderite experiments can be discussed and evaluated as one complete data set. Preliminary calculations performed with the software SUPCRT [4] indicate that the influence of pressure on mineral solubilities – especially for carbonates – is rather negligible (< 1% relative difference) in the range 20-30 MPa, but needs to be considered in the range 0.1-20 MPa. For these differences in pressure thermodynamic databases used for geochemical modeling, e.g., should hence be fitted.

Concentrations of Ca^{2+}, Mg^{2+}, Mn^{2+} and Fe^{2+} in the brine show rapid and steep initial increases followed by slight decreases afterwards (Fig. 1). The initial increases are most likely related to kinetically rapid dissolution of fines (e.g. [5], [6], [7]) present in the untreated siderite separate; possibly due to crushing. Such fines were detectable on grain surfaces of some untreated siderite and ankerite grains (Fig. 2B). Subsequent decreases in ion concentration levels are related to the formation of (a) mineral phase(s) incorporating the respective cations. Note that no newly formed phase(s) were detected. This is most likely related to either subsequent dissolution of the new formed phase(s), or to the fact that the amount of (the) new formed phase(s) was too small to be detected. After reaching a minimum, Ca^{2+} and Mg^{2+} brine

concentrations increase again implying dissolution of Ca^{2+} and Mg^{2+} components to the end of the experiments. In contrast to that, Fe^{2+} and Mn^{2+} concentrations in the samples brine decrease after having reached a maximum. This implies continuous precipitation of (a) mineral(s) incorporating Fe^{2+} and Mn^{2+} ions, respectively. These findings are in line with SEM investigations, which clearly show dissolution of CO_2-exposed ankerite, but minor dissolution features or partially undissolved siderite grains (Fig. 2C).

These latter observations can be explained by kinetically rapid dissolution of Ca^{2+}(/Mg^{2+})-rich ankerite, that, after Ca^{2+} (super)saturation is reached in the brine, changed into precipitation of Fe^{2+}(/Mn^{2+})-rich siderite. As Mg^{2+} is also present in siderite it is furthermore possible that partial dissolution of Mg^{2+} occurs in siderite leaving other ions largely unaffected within the crystal lattice. Another explanation would be the substitution of Mg^{2+} by Fe^{2+} and Mn^{2+} in siderite and/or ankerite. It is known from literature that in siderite Fe^{2+} is replaced by other metallic ions such as Mg^{2+} and Mn^{2+}, but also that the main substitution in ankerite is that of Fe^{2+} for Mg^{2+}, and subordinately for Mn^{2+} [8]. Similar substitution processes in the siderite separate could explain increasing Mg^{2+} opposed to decreasing Fe^{2+} and Mn^{2+} brine concentrations by Mg^{2+} substitution for Fe^{2+} and Mn^{2+} in ankerite (and/or siderite).

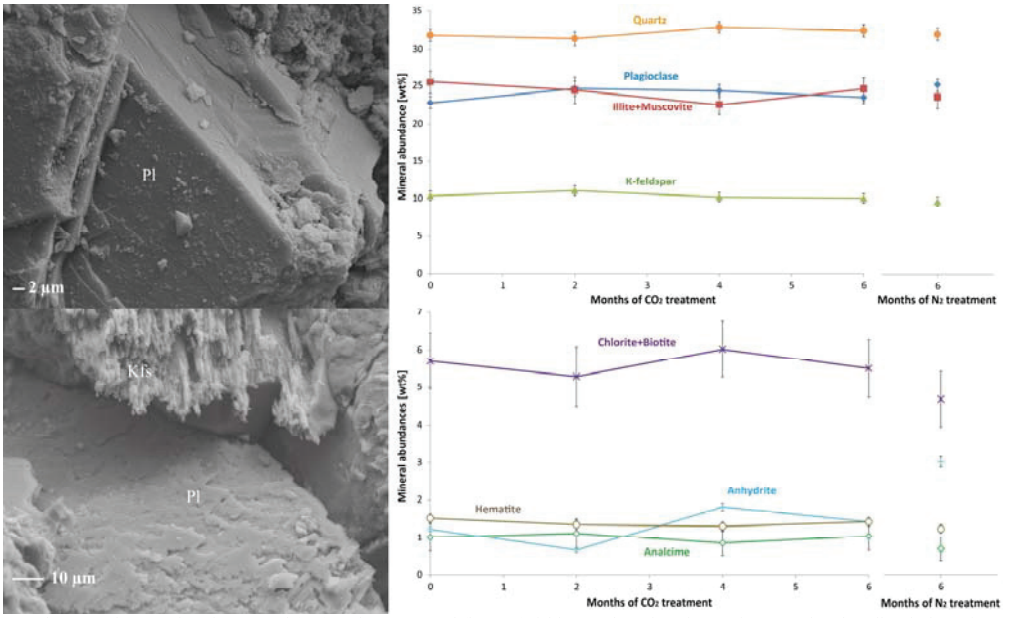

Fig. 5 – Micrographs of untreated (top) and CO_2-treated (bottom) feldspar mineral surfaces of Exp-A showing dissolution of plagioclase (pl) as well as of K-feldspar (Kfs) due to CO_2 exposure. The right side shows two plots of Rietveld refined XRD data of Exp-B for major (top) and minor (bottom) mineral phases of the CO_2- and N_2-treated siltstone, respectively. Changes in mineral abundance are related to the natural variability and not caused by CO_2 exposure.

By performing a reservoir simulation study of geochemical processes occurring within the reservoir of the Ketzin pilot site, [9] found out that siderite is the most stable carbonate mineral trapping phase. Similar observations are described in [10], who performed geochemical modeling using Rotliegend Sandstone and observed dissolution of anhydrite and hematite next to precipitation of iron carbonate at 5 MPa pCO_2. [11] also concluded that in low-temperature (37 °C) Utsira-like reservoirs, the formation of siderite (or hydrous magnesium carbonates) is favored over that of ankerite (and dolomite and magnesite).

The findings of the latter three papers performing numerical experiments are supported by the here presented laboratory experiments, in which ankerite dissolves and siderite is more stable. While e.g. [9] included other carbonates (i.e. calcite, dolomite and magnesite) in their models and conclusions are more robust accordingly, the here used siderite separate only contained ankerite next to siderite as carbonate phases and conclusions regarding carbonate stabilities in general are obsolete. Nonetheless, our results show that siderite is likely to be a stable mineral trapping phase; at least in Fe^{2+}-bearing reservoirs. In contrast to that, [6] and [12] argued that, amongst others, ankerite can replace siderite or precipitate instead of it due to increased Ca^{2+} brine concentrations. Their findings originate from a very specific modeling study. They evaluated geochemical changes in ferric-iron bearing synthetic redbed reservoirs as a consequence of co-injecting CO_2 and sulfur-bearing waste gas. Thermodynamic data for ankerite was not available in the kinetic modeling database. For that reason ankerite was excluded from the mineral assemblages. A comparison of siderite and ankerite stabilities over time is thus missing, and it is concluded that siderite is a major carbonate trapping phase.

Exp-A and Exp-B show only minor changes during long-term CO_2-exposure experiments. In sandstone (Exp-A), major changes are related to feldspar minerals that show (intensified) dissolution with experimental time (Fig. 5). In siltstone, mineral abundances do not reveal significant differences comparing untreated and N_2-treated with CO_2-treated siltstone samples (Fig. 5).

6. Conclusions

The analysis of CO_2-exposure experiments performed on the monomineralic siderite separate show that ankerite is dissolved and siderite is stable. Accordingly, it is likely that siderite is a stable CO_2 trapping phase in Fe-bearing reservoirs.

The experiments on sandstone and siltstone samples from the Ketzin reservoir reveal only minor changes in mineralogy and geochemistry. In sandstone samples, analcime, chlorite, hematite and illite abundances slightly decrease, while quartz abundances tendentially increase with time. Feldspar minerals (plagioclase and K-feldspar) show clear signs of dissolution. In siltstone, changes of mineral abundances are mainly within analytical error. By performing whole rock exposure experiments it is generally difficult to differentiate CO_2-related changes from the natural variability of the samples.

Based on our studies, the chemical integrity of the Ketzin reservoir is not (significantly) affected by the injection of CO_2, and siderite is presumably a stable (long-term) CO_2 trapping phase.

Acknowledgements

The authors gratefully acknowledge funding within the CO_2MAN project by the German Federal Ministry of Education and Research as part of the GEOTECHNOLOGIEN Program (this is publication GEOTECH-2046), and by industry partners. Furthermore, the authors would like to thank Christian Ostertag-Henning from BGR Hannover for sample distribution and fruitful discussions, as well as Burt Thomas and Robert Rosenbauer from USGS at Menlo Park, CA, USA for initiating the GaMin'11 project together with BGR Hannover. We are thankful for technical assistence of Reiner Schulz, Hans-Peter Nabein, Rudolf Naumann, Sabine Tonn, Andrea Gottsche and Ilona Schäpan from GFZ Potsdam.

References

[1] Fischer, S., Liebscher, A., Wandrey, M., and the CO_2SINK Group, 2010. CO_2-brine-rock interaction – first results of long-term exposure experiments at in situ P-T conditions of the Ketzin CO_2 reservoir. Chem. Erde 70, 155–164.

[2] Fischer, S., Zemke, K., Liebscher, A., Wandrey, M., and the CO_2SINK Group, 2011. Petrophysical and petrochemical effects of long-term CO_2-exposure experiments on brine-saturated reservoir sandstone. Energy Procedia (4), 4487–4494.

[3] Kaufhold, S., Dohrmann, R., 2012. Mineral standards for the COORAL project (#COO14 Siderite). Internal Technical Report, BGR Hannover.

[4] Johnson, J.W., Oelkers, E.H., Helgeson, H.C., 1992. SUPCRT92: A software package for calculating the standard molal thermodynamic properties of minerals, gases, aqueous species, and reactions from 1 to 5000 bar and 0 to 1000°C. Computers & Geosciences 18 (7), 899–947.

[5] Palandri, J.K., Rosenbauer, R.J., Kharaka, Y.K., 2005. Ferric iron in sediments as a novel CO_2 mineral trap: CO_2-SO_2 reaction with hematite. Appl. Geochem. 20, 2038–2048.

[6] Holdren, G.R., Berner, R.A., 1979. Mechanism of feldspar weathering. 1. Experimental Studies. Geochim. Cosmochim. Acta 43, 1161-1171.

[7] Bateman, K., Turner, G., Pearce, J.M., Noy, D.J., Birchall, D., and Rochelle, C.A., 2005. Large-Scale Column Experiment: Study of CO_2, Porewater, Rock Reactions and Model Test Case. Oil & Gas Science and Technology – Proceedings of the International Conference on Gas-Water-Rock Interactions Induced by Reservoir Exploitation, CO_2 Sequestration and Other Geological Storage, Vol. 60 (1), 161–175.

[8] Deer, W. A., Howie, R. A., Zussman, J., 1992. An Introduction to the Rock-Forming Minerals (2nd Edition), Prentice Hall, London.

[9] Klein, E., De Lucia, M., Kempka, T., Kühn, M. Evaluation of long-term mineral trapping at the Ketzin pilot site for CO_2 storage: An integrative approach using geochemical modelling and reservoir simulation. Submitted to IJGGC.

[10] De Lucia, M., Bauer, S., Beyer, C., Kühn, M., Nowak, T., Pudlo, D., Reitenbach, V., Stadler, S., 2012. Modeling CO_2-induced fluid-rock interactions in the Altensalzwedel gas reservoir. Part I: From experimental data to a reference geochemical model. Environ. Earth Sci. 67 (2), 563–572.

[11] Pham, V.T.H., Lu, P., Aargaard, P., Zhu, C., Hellevang, H., 2011. On the potential of CO_2-water-rock interactions for CO_2 storage using a modified kinetic model. IJGGC 5, 1002–1015.

[12] Palandri, J.L., Kharaka, Y.K., 2005. Ferric-iron bearing sediments as a mineral trap for CO_2 sequestration: Iron reduction using sulfur-bearing waste gas. Chem. Geol. 217 (3–4), 351–364.